

Precise Subcellular Input Retinotopy and Its Computational Consequences in an Identified Visual Interneuron

Simon P. Peron,^{1,2,*} Peter W. Jones,² and Fabrizio Gabbiani^{2,3,*}

¹Janelia Farm Research Campus, Howard Hughes Medical Institute, 19700 Helix Drive, Ashburn, VA 20147, USA

²Department of Neuroscience, Baylor College of Medicine, One Baylor Plaza, Houston, TX 77030, USA

³Department of Computational and Applied Mathematics, Rice University, 6100 Main, Houston, TX 77005, USA

*Correspondence: perons@janelia.hhmi.org (S.P.P.), gabbiani@bcm.edu (F.G.)

DOI 10.1016/j.neuron.2009.09.010

SUMMARY

The Lobula Giant Movement Detector (LGMD) is a higher-order visual interneuron of Orthopteran insects that responds preferentially to objects approaching on a collision course. It receives excitatory input from an entire visual hemifield that anatomical evidence suggests is retinotopic. We show that this excitatory projection activates calcium-permeable nicotinic acetylcholine receptors. In vivo calcium imaging reveals that the excitatory projection preserves retinotopy down to the level of a single ommatidium. Examining the impact of retinotopy on the LGMD's computational properties, we show that sublinear synaptic summation can explain orientation preference in this cell. Exploring retinotopy's impact on directional selectivity leads us to infer that the excitatory input to the LGMD is intrinsically directionally selective. Our results show that precise retinotopy has implications for the dendritic integration of visual information in a single neuron.

INTRODUCTION

Several lines of investigation have contributed to our understanding of the impact spatial structure has on synaptic integration: work on the role of neuronal morphology (Schaefer et al., 2003; Krichmar et al., 2002; Vetter et al., 2001), synapse position (Williams and Stuart, 2003; Spruston et al., 1994; Rall, 1970; Rall et al., 1967), and the spatial distribution of active conductances (Johnston and Narayanan, 2008; Migliore and Shepherd, 2002; Johnston et al., 1996). These approaches have demonstrated that synaptic integration cannot be understood outside of the spatial context (Spruston, 2008). Consequently, the spatial layout of the projections a neuron receives will impact synaptic integration. Specifically, dendrites that receive inputs from a topographically structured projection of axons will be uniquely situated to perform computations on whatever stimulus variable is topographically represented. Such computations have been postulated in several systems. In the retina, the relative position

of inhibitory and excitatory synapses on the dendrites of starburst amacrine cells may play a role in directional selectivity (Hausselet et al., 2007; Euler et al., 2002). Additionally, dendritic asymmetry is thought to underlie the directional preference of certain classes of retinal ganglion cells (Kim et al., 2008; but see Chen and Chiao, 2008). In the fly, the receptive field of lobula plate tangential cells (LPTCs) is partly determined by their position within the topographically organized lobula plate (Krapp et al., 1998; Haag and Borst, 2004). In visual cortex, it has been suggested that orientation selectivity can be explained by dendritic orientation (Colonnier, 1964; but see Martin and Whitteridge, 1984).

In all these cases, however, the topography of subcellular wiring remains poorly understood. Though an initial examination of wiring in LPTCs (Borst and Egelhaaf, 1992) was consistent with retinotopy, this input has not yet been examined systematically. Indeed, most studies of mapping topography focus on wiring at the circuit level (Garel and Rubenstein, 2004; Ruthazer and Cline, 2004; Strausfeld and Nüssel, 1981), and connectivity is inferred from axon-dendrite overlap (Stepanyants and Chklovskii, 2005; Stepanyants et al., 2004). Studying functional subcellular wiring is technically challenging; to establish the presence of functional synapses, one has to simultaneously stimulate subsets of input axons and measure the dendritic position of postsynaptic responses. While recent work has demonstrated a coarse-level mapping in the optic tectum of zebrafish (Bollmann and Engert, 2009), and technical advances have permitted the study of subcellular input organization in cortex (Petreanu et al., 2009), it remains to be determined whether topography is preserved at the fine scale, and whether it has the theoretically predicted computational consequences (Rall 1970).

The Lobula Giant Movement Detector (LGMD) is a large visual interneuron found in the lobula of Orthopteran insects (Gabbiani et al., 2004; O'Shea and Williams, 1974). It is three synapses removed from the photoreceptors, receiving ~15,000 excitatory inputs from an entire visual hemifield. Recent work demonstrates that it lacks dendritic voltage-gated calcium channels (VGCCs) (Peron and Gabbiani, 2009a). Fly LPTCs lie in a relatively similar anatomical position and are known to pass calcium through ionotropic receptors (Oertner et al., 2001; see also: Thany et al., 2007; Oertner et al., 1999). This suggests that the topographic projection from visual space to the LGMD's dendrites could be

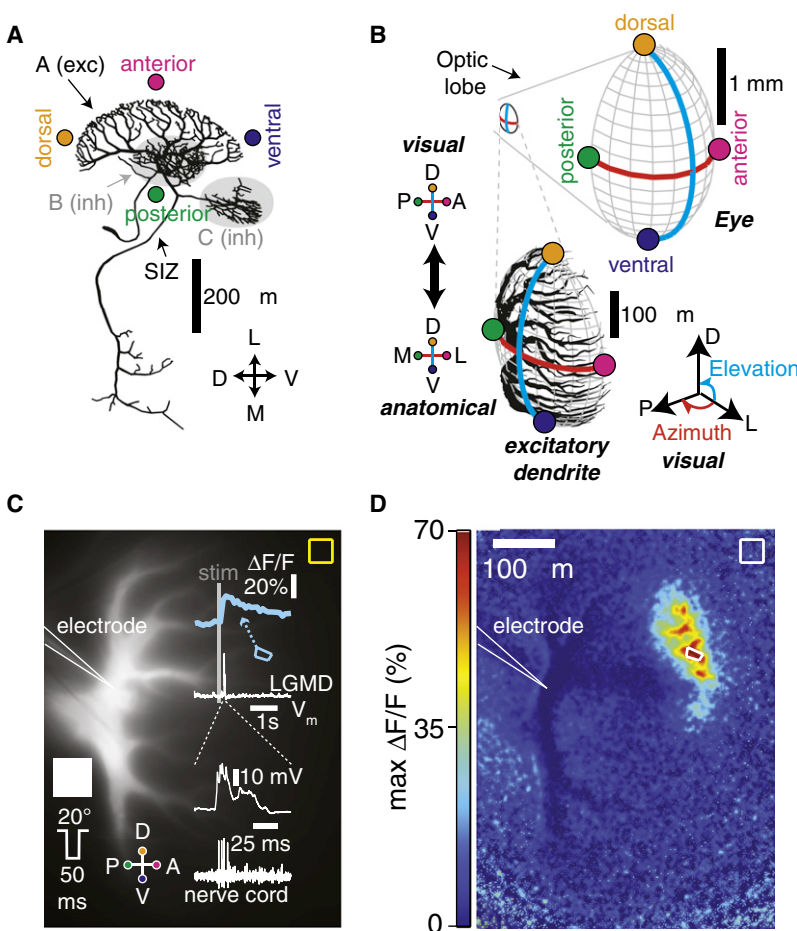


Figure 1. Ca^{2+} Response in the LGMD's Excitatory Dendrite following Localized Visual Stimuli

(A) Reconstructed LGMD (adapted from Peron et al., 2007). Arrows indicate anatomical directions (dorsal, ventral, medial, and lateral). Colored text and dots indicate position in visual space of impinging synaptic input.

(B) The morphology of the LGMD approximates that of the locust eye, both of which are shown to scale at top. Colored text and dots near eye denote position in visual space. The red line denotes the equator (elevation = 0°), along which azimuth is measured; azimuth = 0° at the anterior pole. Elevation varies along the blue line; the red and blue lines intersect at elevation = 0° and azimuth = 90° . Arrows denote dorsal, lateral, and posterior in visual space, illustrating measurement of azimuth and elevation angles. The projection from visual space to LGMD anatomical space is shown in the left inset; visual anterior, posterior, dorsal, and ventral correspond to anatomical lateral, medial, dorsal, and ventral, respectively. Throughout, the visual coordinates of synaptic inputs will be employed.

(C) Image of an OGB-1-filled LGMD neuron employed in a visual stimulation experiment (stimulus: 50 ms OFF flash of a 20° -by- 20° square). Yellow region was used for background subtraction while cyan denotes the ROI used to calculate the $\Delta F/F$ trace shown in the same color. A gray line depicts stimulus timing. Intracellular V_m is shown on the timescale of the $\Delta F/F$ time series, as well as in a magnified form with the corresponding nerve cord recording. Colored dots (anterior, posterior, dorsal, ventral) correspond to the position in visual space of the incoming inputs from the eye.

(D) Maximal $\Delta F/F$ at each pixel in (C) following stimulus presentation.

assayed directly by combining calcium imaging with visual stimulation.

The LGMD responds preferentially to stimuli on a collision course with the animal (i.e., looming stimuli; Matheson et al., 2004; Gabbiani et al., 2002; Rind and Simmons, 1992; Schlotterer, 1977). Its response to these stimuli as well as its output projections suggests that it is involved in flight and jumping behaviors (Fotowat and Gabbiani, 2007). Specifically, the LGMD outputs in a one-to-one spikewise fashion to the descending contralateral movement detector (DCMD), which has the largest axon in the locust nerve cord and projects to motor centers involved in flight and jumping (Burrows, 1996). Due to the reproducibility of the looming response and its presumed ethological significance, the LGMD is considered a model system for single-neuron computation (London and Häusser, 2005). The precise visual sampling carried out by the locust eye has been measured directly (Krapp and Gabbiani, 2005), and the impact of various projection schemes from visual space to the LGMD's dendrites has been explored in a model (Peron et al., 2007). The presumed layout of the retinotopic projection suggests that each excitatory dendritic branch receives inputs from ommatidia sampling similar elevations in visual space, whereas inputs from a given azimuth activate different branches. This makes the system ideal for the study of interbranch versus

intrabranched synaptic integration (Losonczy and Magee, 2006; Poirazi et al., 2003; Cash and Yuste, 1999).

In this work, we begin by demonstrating that visual stimuli elicit reliable, localized calcium responses in the excitatory dendrite. After establishing the validity of our mapping approach, we systematically measure the projection from visual space to the LGMD's dendrites at several scales. Finally, we investigate the implications of this mapping on the processing of static and dynamic stimuli in the LGMD, using a combination of simulation and in vivo experimentation.

RESULTS

Nature of the Calcium Response in the Excitatory Dendrite

The LGMD has three dendritic fields: one receiving excitatory input (A; Figure 1A), and two receiving inhibitory input (B, C). The anatomical structure of field A is illustrated in relation to the eye anatomy in Figure 1B. This dendritic field has an ellipsoidal geometry that, rotated 90° about its major axis, matches the eye geometry (Peron et al., 2007). This suggests that the elevation of a visual stimulus along the eye is represented along the major axis of the ellipsoid in dendritic space while azimuth lies along the equator (blue and red curves, respectively,

Figure 1B). In this scheme, inputs from anterior visual space synapse onto the anatomically lateral tips of the excitatory dendrite, while inputs from posterior visual space will synapse onto anatomically medial proximal dendritic segments. Inputs from dorsal and ventral visual space should project onto the anatomically dorsal and ventral segments of the excitatory dendrite, respectively.

To study the topography of projections onto the excitatory dendritic tree, a method for determining the position of functional synapses is necessary. In earlier work, we established that depolarization of the excitatory dendrite did not elicit dendritic calcium influx (Peron and Gabbiani, 2009a), implying the absence of dendritic VGCCs. If the ionotropic receptors on this dendrite are calcium permeable and the calcium influx is spatially confined, calcium could be used as an indicator of synaptic position. Because anatomical evidence suggests that the excitatory dendrite receives cholinergic inputs (Rind and Leitinger, 2000; Rind and Simmons, 1998), we iontophoretically puffed acetylcholine (ACh; 1M) onto the excitatory dendrite after filling the LGMD with the calcium indicator Oregon Green BAPTA-1 (OGB-1). Relative fluorescence ($\Delta F/F$) increased in response to ACh at sites proximal to the puffing electrode, while a site only $\sim 75 \mu\text{m}$ further away showed no response (Figure S1, available online), suggesting the presence of calcium-permeable cholinergic receptors.

To differentiate between nicotinic and muscarinic receptors (nAChRs and mAChRs, respectively), we repeated the experiment with the nAChR antagonist mecamylamine (1 mM). The maximal $\Delta F/F$ response declined following mecamylamine application ($n = 5$ cells; $p = 0.008$ Wilcoxon rank sum test; mean decline of 82%). No decline was observed over the same time period in control animals ($n = 5$ cells; $p = 0.69$; Figure S1). In combination with our previous results pointing to the lack of VGCCs, this implies that the calcium signal was primarily due to direct calcium influx through nAChRs, and not due to secondary release caused by mAChRs (e.g., David and Pitman, 1996). Though we did not test for internal store-based calcium-induced calcium release (Verkhratsky and Shmigol, 1996), the limited spatial extent of the calcium response suggested that we could resolve synaptic position even if such release occurs.

Because calcium influx was likely a direct reflection of synaptic activity, we examined calcium influx in the context of visual stimulation. A variety of stimuli were tested (Experimental Procedures), each producing a spatially localized calcium response consistent with anatomical predictions (Figure S2). Figure 1C shows the $\Delta F/F$ response to a 50 ms, 20° -by- 20° OFF square stimulus, along with concurrent intracellular LGMD and extracellular nerve cord recordings. The calcium influx was highly localized (Figure 1D). Of the range of stimuli tested, the strongest responses were obtained with 2 s, 10° -by- 10° and 50 ms, 20° -by- 20° OFF squares, while the weakest were obtained with 50 ms, 10° -by- 10° squares with a 10% luminance decrease and 50 ms, 5° -by- 5° OFF squares (Figure S2). Larger sizes and luminance changes always produced stronger $\Delta F/F$ responses, and longer duration stimuli produced either similar or stronger responses. Maximal $\Delta F/F$ and the peak firing rate were significantly correlated only for posterior stimuli, presumably due to the greater proximity of the posterior position to the spike initia-

tion zone (SIZ) (mean $\rho = 0.35$ across $n = 5$ animals, $p < 0.05$; slope: 22 spikes/s / % $\Delta F/F$). In animals ($n = 2$; see Experimental Procedures) where concurrent intracellular recording and imaging was performed, maximal $\Delta F/F$ correlated with peak voltage deflection ($\rho = 0.28$, $p < 0.01$; $n = 237$ trials, 25 positions per animal). Time-to-peak (10% to 90%) for the membrane potential response was 14.2 ± 1 ms, while the calcium signal peaked, on average, in 150 ± 21 ms (mean \pm SEM; see also Figure 1C).

Preservation of Coarse Retinotopy in the Excitatory Dendrites

Having established that calcium imaging provides a reliable indication of synapse position, we next characterized coarse retinotopy in the excitatory dendrites. Animals were presented with 25 equally spaced 20° -by- 20° , 50 ms OFF stimuli in a 100° -by- 100° region of visual space. The maximal $\Delta F/F$ response was measured at each pixel, and pixels attaining at least 85% of the maximal overall response were retained and pooled across imaging depths (Figure 2A; see Experimental Procedures for explanation of threshold selection). For each stimulus position, the center of mass (COM) of this set of pixels was determined (Figure 2B). Because the excitatory synapses are known to habituate (O'Shea and Rowell, 1976), and because we wished to image at multiple depths, it was important to establish that a limited number of measurements would provide an accurate assessment of topography. We examined the variability in the COM's position for stimuli imaged at the same depth over time, observing a COM standard deviation (SD) of 7.9 and $12.3 \mu\text{m}$ for the medial-lateral and dorsal-ventral (DV) directions, respectively ($n = 5$ animals with ≥ 5 trials per animal to obtain individual SDs; Figure S3). We observed a comparable COM positional variability when imaging across depths, with an average COM SD of 9.5 and $9.2 \mu\text{m}$ for the medial-lateral and DV directions, respectively ($n = 59$: 7 animals, ~ 8 positions each, with ≥ 5 trials per animal-position combination to obtain individual SDs). Thus, COM position was stable across time and depth.

To quantify the degree of visual topography preservation, we counted the number of times each COM's position violated retinotopy relative to other COMs whose visual stimuli shared its elevation or azimuth (see Experimental Procedures and Figure S4). As indicated in Table 1, 391 out of 392 comparisons were correct, demonstrating a high degree of topography preservation. We constructed a cross-animal topography by placing the COMs in a coordinate system centered on the excitatory dendritic field's origin, normalized to the span of each excitatory dendritic field along its major axis, and rotated so that the major axis would be vertical (Figure 2C; $n = 7$ animals). The mean length of the major axis of the dendritic field was $384.5 \pm 31.6 \mu\text{m}$ ($n = 7$ cells; mean \pm SEM). In the averaged map, all COMs obeyed the expected topography.

Anatomy suggests that the excitatory dendrite receives distinct ON and OFF input from each ommatidium (Strausfeld and Nässel, 1981). Furthermore, the locust eye samples the visual equator disproportionately (Krapp and Gabbiani, 2005). Simulations show that under the assumptions of retinotopy and constant synaptic density, synapses receiving equatorial inputs occupy more space along the DV axis than synapses

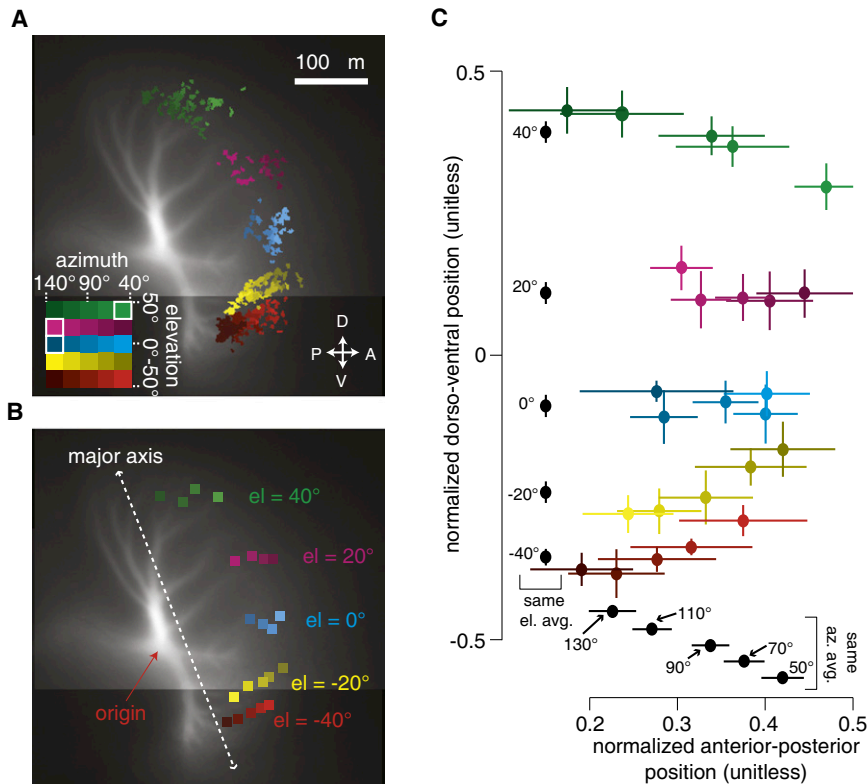


Figure 2. The Excitatory Dendritic Field's Inputs Preserve the Topography of Visual Space at the Coarse Scale

(A) Raw responses to distributed stimuli in a sample LGMD neuron. OFF stimuli were employed across a 100° -by- 100° area divided into a grid of 25 20° -by- 20° squares. The inset color code matches the color of the fluorescence response superimposed over the raw fluorescence image (coordinates are in visual space; positions eliciting no response are outlined in white). At each of five depths, pixel groups meeting our 85%, 10 connected pixels criteria were recorded (see [Experimental Procedures](#)); each colored area corresponds to the union of such groups across depths and fields of view for a particular stimulus site. Directional arrows correspond to the position in visual space of the incoming inputs from the eye (see [Figure 1](#)).

(B) COMs for the responding regions shown in (A). The dendritic field's origin and major axis are indicated with red and dotted white lines, respectively.

(C) Normalized COM positions across cells ($n = 7$; lines indicate SEM). The black points indicate the normalized positions of all points with a given azimuth or elevation.

receiving input further from the equator ([Peron et al., 2007](#)). We did not observe a systematic increase in inter-COM distance toward the equator, suggesting that the input onto the LGMD compensates for the sharp decline in ommatidial density along the equator ([Figure 2C](#), black dots along DV axis). This result is consistent with the observation of stronger responses to inputs further from the equator than predicted by ommatidial density alone ([Krapp and Gabbiani, 2005](#)). We examined the alignment of the ON and OFF inputs onto the LGMD by applying COM displacement analysis to the 2 s ON and OFF stimuli from [Figure S2](#). The displacements in the medial and ventral directions of 10.9 ± 6.2 and 7.5 ± 7.2 μm (mean \pm SEM), respectively, were within the range of positional SD obtained above, and not statistically significant ($n = 25$ trial pairs over 5 animals, $p = 0.23$ and 0.08 , respectively; Wilcoxon signed rank test). These results imply a precise overlap of the ON and OFF pathways.

Preservation of Fine Retinotopy in the Excitatory Dendrites

We examined fine-scale retinotopy, using 0.5° -by- 0.5° , 50 ms ON stimuli spaced 2° apart. These stimuli should activate single, adjacent ommatidia, based on the distribution of ommatidial optical axes ([Krapp and Gabbiani, 2005](#)) and acceptance angles ([Wilson, 1975](#)). The peak depolarization observed in response to this ON stimulus was smaller than the response to the 20° -by- 20° OFF stimuli employed in the coarse mapping ($p < 0.01$, Wilcoxon rank sum test; $n = 150$ and 23 trials for 0.5° -by- 0.5° and 20° -by- 20° stimuli, respectively). To directly confirm that these stimuli activated single ommatidia, we compared the response

to those obtained using an apparatus specifically designed to stimulate single ommatidia ([Experimental Procedures](#)). The peak depolarizations elicited by 0.5° -by- 0.5° ON mapping stimuli were indistinguishable from those evoked using the single-ommatidial stimulation apparatus ($p = 0.99$, Wilcoxon rank sum test; $n = 10$ ommatidia and 150 0.5° -by- 0.5° ON trials). In addition, the time course of the mean mapping stimulus response fell within the SEM of the mean response evoked by the single-ommatidial apparatus ([Figure 3A](#)). To determine how many presynaptic LGMD afferents single-ommatidial stimulation activated, we compared the peak excitatory postsynaptic currents (EPSCs) evoked by light stimulation using the single-ommatidial apparatus with spontaneous EPSCs ([Figure S5](#)). This analysis revealed that light activation of a single ommatidium corresponds to the activation of five to six presynaptic LGMD afferents, a number consistent with activation of an afferent with a receptive field centered on the stimulated ommatidium, along with its immediately adjacent afferents.

As with the coarse mapping, we applied the 85% threshold on maximum $\Delta F/F$ responses to obtain pixels responding to our 0.5° -by- 0.5° ON stimuli ([Figure 3B](#)). Analysis of the COMs revealed that even at this finest of scales, retinotopy was highly preserved ([Figure 3C](#); [Table 1](#)). Intermediate stimuli, consisting of four adjacent 10° -by- 10° , 50 ms OFF squares in a 20° -by- 20° region, as well as four adjacent 5° -by- 5° , 50 ms OFF squares in a 10° -by- 10° region, also obeyed retinotopy ([Figure S6](#)), as did 0.5° -by- 0.5° , 50 ms ON stimuli spaced 4° apart ([Figure S7](#)).

To determine whether the positional errors were a consequence of measurement noise, we examined the variability in

Table 1. Degree of Retinotopy Preservation across All Stimulus Classes

Stimulus Size	Inter-COM Distance (Mean \pm SD; μm)			Basal Variability for COM Position (μm)		Number of COM Comparisons (% Below Noise Threshold in Paren.)			n_{animals}
	along ML axis	along DV axis	combined	SD along ML axis	SD along DV axis	retinotopy preserved	retinotopy violated	percent correct	
Adjacent COMs only									
0.5°-by-0.5° 2° spacing	9.2 \pm 8.1	13.4 \pm 11.3	11.4 \pm 10.1	2.4 (n = 18)	5.5 (n = 18)	111	30 (83%)	78.7%	4
0.5°-by-0.5° 4° spacing	7.9 \pm 5.6	20.0 \pm 11.9	14.0 \pm 11.1	2.4 (n = 27)	6.3 (n = 27)	167	19 (95%)	89.8%	5
5°-by-5°	9.5 \pm 6.7	20.9 \pm 13.0	15.3 \pm 11.8	5.7 (n = 25)	5.5 (n = 18)	28	11 (100%)	71.8%	5
10°-by-10°	16.0 \pm 15.4	35.0 \pm 36.3	25.5 \pm 29.4	3.1 (n = 18)	2.9 (n = 18)	50	10 (60%)	83.3%	5
20°-by-20°	21.3 \pm 10.4	70.4 \pm 28.4	44.6 \pm 32.3	8.7 (n = 57)	7.5 (n = 57)	172	1 (100%)	99.4%	7
Nonadjacent and adjacent COMs									
0.5°-by-0.5° 2° spacing	–	–	–	2.4 (n = 18)	5.5 (n = 18)	311	40 (78%)	88.6%	4
0.5°-by-0.5° 4° spacing	–	–	–	2.4 (n = 27)	6.3 (n = 27)	437	26 (88%)	94.3%	5
20°-by-20°	–	–	–	8.7 (n = 57)	7.5 (n = 57)	391	1 (100%)	99.7%	7

The top set of numbers—adjacent COMs only—refers to measurements using *only* points adjacent in visual space; the bottom set includes spatially adjacent and nonadjacent COMs. The leftmost column gives the size of the stimulus. The next three columns give the distance between adjacent COMs (mean \pm SD, in μm) along the medial-lateral (ML) anatomical axis (this corresponds to the anterior-posterior, or AP, axis in visual space), dorsal-ventral (DV) anatomical axis, and a pooling of the two, respectively. The next two columns show the mean COM position SD (in μm) for each stimulus across animal-position pairings (individual SDs obtained from animal-position pairings with at least five trials). The first of these gives the variability along the ML anatomical axis (AP visual axis), while the second gives variability along the DV axis. The next two columns give the number of comparisons at each scale that preserved or violated retinotopy, with the percent of point pairs whose interpoint distance was below the $3.46 \cdot \sigma$ distance threshold given in parentheses for retinotopy violators (see [Experimental Procedures](#)). Retinotopy violations for pairs below threshold are most likely due to measurement noise (σ is the mean of the two SDs in the fourth and fifth columns). The final two columns give the percentage of correct retinotopy comparisons, and the number of animals employed for each stimulus class, respectively.

COM position for stimuli having the same size as the ones employed for the mappings, and compared this to the distance between pairs of COMs that did not preserve retinotopy correctly. This allowed us to define a noise threshold ([Experimental Procedures](#)) and test whether erroneous relationships were disproportionately observed with subthreshold inter-COM distances. As [Table 1](#) shows, this turned out to be the case for all stimulus classes. At the lowest stimulus size and spacing, the fraction of retinotopy violations that were above the noise threshold amounted to 17% (first row of [Table 1](#)), suggesting that this is the fraction of violations due to discontinuities in the map imposed by dendritic architecture. The average distance between neighboring COMs correlated strongly with stimulus spacing, both along elevation ($\rho = 0.997$, $p = 1.9 \times 10^{-4}$) and azimuth ($\rho = 0.967$, $p = 0.007$), suggesting a highly linear transform between visual space angular coordinates and the dendritic field Euclidean coordinates. Visual space was more compressed along azimuth ($1.6 \mu\text{m}/^\circ$) than along elevation ($3.9 \mu\text{m}/^\circ$). Overall, our results show that retinotopy preservation exists at even the finest scale measured.

Computational Consequences of Retinotopy: Response to Static Stimuli

Our mapping data imply that visual stimuli spanning the same elevation will tend to activate the same dendritic branches, while stimuli spanning the same azimuth will activate different branches.

Using COMs projected onto 3D reconstructions of the excitatory dendrites ([Figure S8](#)), we found that the distance along the dendrites between two projected COMs was $198.0 \pm 10.3 \mu\text{m}$ (mean \pm SEM, $n = 96$ distances) when their corresponding visual stimuli had the same elevation, but $389.5 \pm 7.0 \mu\text{m}$ ($n = 121$) when they had the same azimuth ($p = 3.1 \times 10^{-28}$, Wilcoxon rank sum test). This suggested that the LGMD could indeed be used to examine clustered versus distributed synaptic activation.

We presented the LGMD/DCMD with flashing, 50 ms OFF bar stimuli that were either horizontal, activating clustered synapses, or vertical, activating distributed synapses ([Figure 4A](#), top). We observed a larger maximal firing frequency (f_{max}) response when presenting vertical 80° -by- 5° bars relative to horizontal bars ([Figure 4A](#)). We confirmed that this result was consistent with cable theory by presenting the same stimuli in a model of the LGMD. The model combined previous simulations ([Peron and Gabbiani, 2009b](#)) with the sampling density of the locust eye ([Krapp and Gabbiani, 2005](#)) and the mapping from visual space to the dendrites obtained here. This yielded the same preference for vertical over horizontal stimuli ([Figure 4B](#)). Since the sublinear summation effect depends on having disparate versus clustered synapses, we conjectured that smaller bars should result in a less pronounced effect. This was confirmed in vivo, where 20° -by- 5° bars resulted in vertical preference, but 10° -by- 2.5° bars did not ([Figure 4C](#), [Table S1](#) available online). In the model, the preference was abolished for 20° -by- 5° bars and

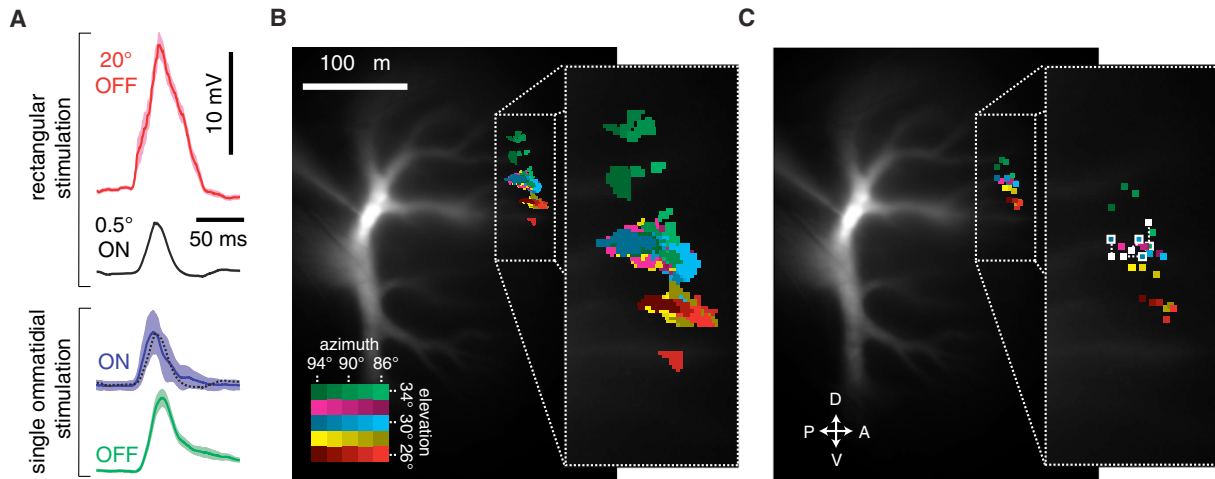


Figure 3. The Excitatory Dendritic Field's Inputs Preserve the Topography of Visual Space at the Fine Scale

(A) 50 ms, 0.5°-by-0.5° ON stimulus produces a response that is indistinguishable from single-ommatidial stimulation. From top to bottom: V_m response to 20°-by-20° OFF (red; $n = 23$ presentations, four sites), 0.5°-by-0.5° ON (black; $n = 150$ presentations, 25 sites), single-ommatidial ON (blue; with 0.5°-by-0.5° response superimposed; $n = 10$ ommatidia), and OFF (green; $n = 19$ ommatidia) stimulation with SEM envelopes.

(B) Raw fluorescence responses to fine-scale stimuli. The color in the stimulus-position-indicating inset corresponds to the color of the fluorescence response. Actual stimuli were 0.5°-by-0.5°, with a 2° centerwise spacing between adjacent sites. The 85% threshold employed in Figure 2A was applied here.

(C) COMs for the responding regions shown in (B). Points (4/25) violating retinotopy are outlined in white, with position shifts that would result in retinotopy preservation indicated. Directional arrows correspond to the position in visual space of the incoming inputs from the eye (see Figure 1).

10°-2.5° bars. Thus, the LGMD conforms to predictions of passive cable theory in the context of static stimuli.

Computational Consequences of Retinotopy: Response to Dynamic Stimuli

We next examined the response of the LGMD/DCMD to translating stimuli by presenting the animal with 10°-by-10° translating squares moving at 40°/s in anterior-posterior (AP), posterior-anterior (PA), DV, and ventral-dorsal (VD) directions, at an elevation of 0° for AP/PA motion and an azimuth of 90° for DV/VD motion. Such translation produces an onset transient followed by a period of reduced, sustained firing (Figure 5A; Peron and Gabbiani, 2009a). We examined the directional selectivity of both the maximal frequency (f_{max}) and the steady state frequency (f_{ss}) for AP versus PA and DV versus VD motion by computing a directionality index (see Experimental Procedures). Our results revealed a significant preference for AP over PA motion, as well as a significant DV preference (Figure 5B; Table S2). Thus, the LGMD exhibits directional selectivity to translating motion.

We employed our model to test whether these results were consistent with the synaptic mapping. The model yielded different directional selectivity from that observed in vivo (Figures 5C and 5D; Table S2). Specifically, f_{max} was higher for PA than AP motion. This is because posterior inputs are more proximal to the SIZ. Indeed, in vivo posterior stimuli elicit stronger responses than anterior ones (Krapp and Gabbiani, 2005; see also Peron et al., 2007). Furthermore, because DV and VD motion begin and end at positions roughly equidistant from the SIZ, the in vivo DV/VD directional bias observed for f_{ss} was not observed in the model.

Directional Selectivity Is Presynaptic to the Excitatory Inputs

One mechanism that would explain the inconsistency between the model and physiological responses to translating motion is directional selectivity presynaptic to the LGMD, specifically, a preference for AP and DV motion at the level of the inputs. To evaluate this possibility, we started by examining the response to drifting gratings confined to a 20°-by-20° region (Figure 6A). We presented 40°/s drifting gratings for all motion directions at four positions, observing a significant directional preference for both AP over PA and DV over VD motion at the level of f_{max} (Figure 6B; Table S2).

To determine whether directional preference was presynaptic or postsynaptic, we examined calcium influx during the presentation of drifting gratings in the same animals (Figure 6D). At all positions tested, we observed a directional preference for AP over PA and DV over VD motion in the maximal $\Delta F/F$ response, a result consistent with presynaptic directional selectivity (Figure 6E; see Table S2). To determine whether presynaptic directional selectivity could explain the discrepancy between our model and the physiological response to translating squares (Figure 5), we endowed the model with preference for both AP and DV motion. The revised model produced responses that were more consistent with those observed in vivo (Figure S9; Table S2): in response to translating squares, the model responded more strongly to AP relative to PA motion, and DV over VD motion. We also examined the model's response to simulated drifting gratings. While the model without presynaptic directional preference failed to produce substantial directional preference, our revised model produced a preference for both AP relative to PA and DV relative to VD motion.

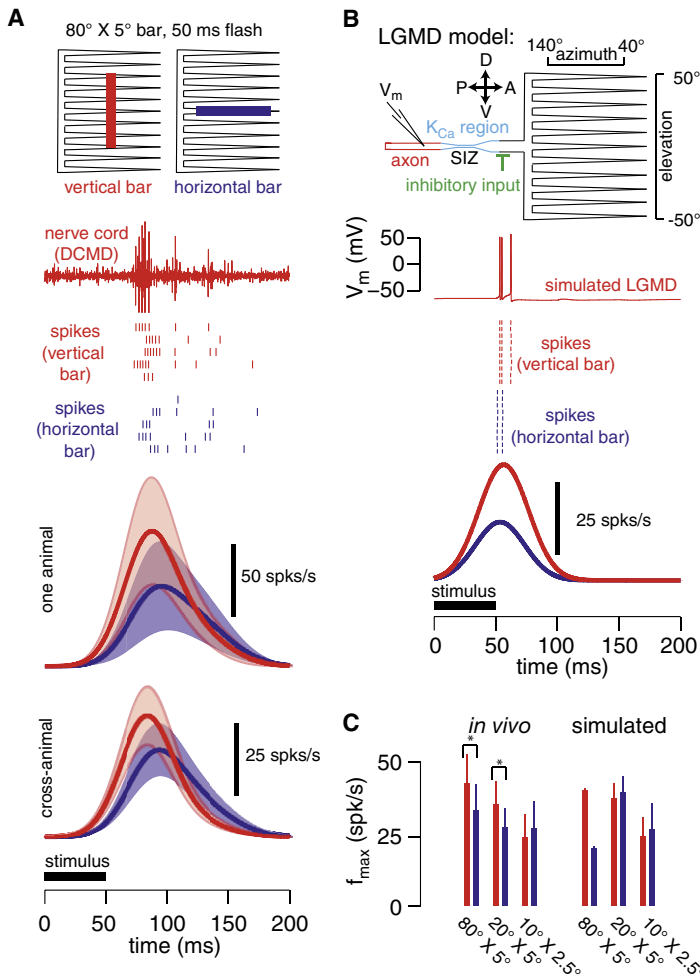


Figure 4. The LGMD Responds More Strongly to Appearing Vertical Bars than Horizontal Bars

(A) In vivo response to 80°-by-5° bar stimuli (50 ms OFF). A schematic of the LGMD excitatory dendritic field is shown with expected positions of synapses activated by vertical (red) and horizontal (blue) bars. Below, the nerve cord response to a single 50 ms OFF presentation of a vertical bar is depicted, above rasters for five trials of vertical and horizontal bars. The Gaussian-convolved ($\sigma = 20$ ms) mean instantaneous frequency response for the animal for which rasters ($n = 5$ trials) are shown and the cross-animal ($n = 43$ trials, pooled over seven animals) average are depicted with envelopes indicating response SEM. Stimulus timing is indicated at the bottom of the panel.

(B) Response of simulated LGMD to 80°-by-5° bar stimuli. The top inset shows the model, which consisted of a spiking axon (red), a region for K_{Ca} -mediated spike-frequency adaptation (blue), feedforward inhibitory input (green), and an excitatory dendrite receiving input from visual space as indicated (see *Experimental Procedures*). The directional arrows (anterior, posterior, dorsal, ventral) correspond to the orientation in visual space of the incoming inputs from the eye (see *Figure 1*). A sample response to a vertical bar presentation is shown below, with rasters for 10 trials each of horizontal and vertical bars following. Finally, the Gaussian-convolved mean instantaneous frequency response across simulations is shown, with light shading indicating SEM.

(C) Summary data for in vivo and simulated response for various bar sizes. Maximal instantaneous frequency (f_{max}) responses for vertical and horizontal bar responses are shown in red and blue, respectively. An asterisk (*) denotes a significant difference in horizontal versus vertical bar response at the $p < 0.05$ level (Wilcoxon signed rank test; see *Table S1*; simulated data not tested).

Because the excitatory dendrite lacks VGCCs, implying that maximum $\Delta F/F$ reflects a response prior to dendritic filtering, while f_{max} provides a dendrite-filtered response, we could evaluate the contribution of dendritic filtering to directional preference directly using our drifting grating stimuli. Specifically, one would expect the 20°-by-5° vertical bars presented during AP/PA drift to activate synapses on disparate branches, while horizontal bars presented during DV/VD drift should activate more clustered synapses. If orientation preference is indeed a result of dendritic sublinear summation, one would expect a decline in response in the context of strong, clustered synaptic activation following dendritic filtering. That is, the $\Delta F/F$ response for a direction producing strong, clustered synaptic activation relative to the $\Delta F/F$ response for other directions should exceed that direction's f_{max} response relative to the f_{max} response to other motion directions. To this end, the responses were normalized to the maximal response for a given animal-position combination, allowing direct comparison of $\Delta F/F$ and f_{max} (*Table S3*). While the normalized f_{max} response was smaller than the normalized $\Delta F/F$ response for all four motion directions, the response decline for DV motion was both the largest and the only statistically significant one, consistent with sublinear summation. This is because

sublinear summation requires not only clustered synaptic activation (an effect both DV and VD motion should have), but also sufficiently strong activation to enter the sublinear regime, explaining the ability of DV, and not VD, motion to produce a significant response decline (DV motion, due to presynaptic directional preference, elicits a stronger depolarization than VD motion). This last result corroborates the orientation preference result from *Figure 5*.

DISCUSSION

The results presented here demonstrate that the LGMD receives a precise retinotopic projection from the locust compound eye. We also demonstrated that the LGMD conforms to cable theoretic predictions, both in terms of its response to clustered and distributed synaptic activation, and in terms of the response to stimuli proximal and distal to the site of spike initiation. We also discovered, due to the inconsistencies between the physiology and simulations, that the neuron receives directionally selective input.

Topography-preserving projections are a ubiquitous feature of nervous systems (e.g., *Garel and Rubenstein, 2004; Ruthazer and Cline, 2004; Strausfeld and Nässel, 1981*). Examinations of subcellular connectivity have, however, usually focused on potential synapses, defined by axon-dendrite overlap (*Stepanyants and Chklovskii, 2005; Jacobs and Theunissen, 2000; 1996*). This is due to the technical difficulty of detecting functional synapses, a task for which calcium imaging is well suited.

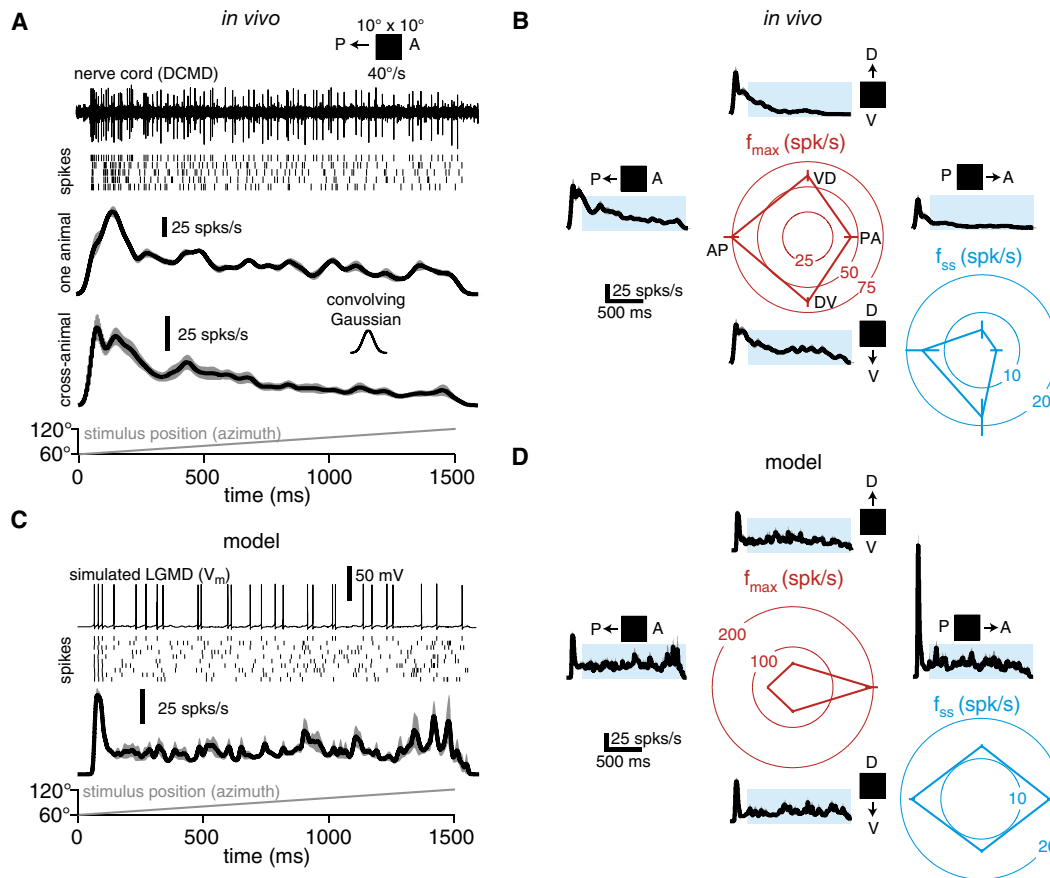


Figure 5. The LGMD Exhibits Directional Selectivity to Translating Motion that Cannot Be Explained by the Organization of the Synaptic Projection Alone

(A) LGMD-DCMD response to translation by a black 10° -by- 10° square moving in an AP direction at $40^\circ/\text{s}$. The top trace shows a sample nerve cord recording, with spike rasters below. The Gaussian-convolved ($\sigma = 20$ ms) mean instantaneous frequency response for the animal for which rasters ($n = 5$ trials) are shown and the cross-animal ($n = 35$, five trials per animal) average are shown with SEM envelopes. The azimuth of the translating square's center is indicated below; elevation was always 0° .

(B) Directional selectivity at the level of maximal frequency (f_{\max} ; red) and steady-state frequency (f_{ss} ; blue) for translating stimuli moving in the AP, PA, DV, and DV directions. Each circular plot indicates f_{\max} or f_{ss} for each of the four stimulus directions, with lines indicating SEM across animals ($n = 7$). f_{ss} was defined as the mean frequency from 250 ms after motion onset to motion termination (light blue; $n = 35$, five per animal).

(C) Simulated LGMD's response to a 10° -by- 10° square translating in an AP direction at $40^\circ/\text{s}$. A sample response is shown with raster plots for 10 trials. The Gaussian-convolved mean instantaneous frequency response is shown below ($n = 10$ trials), with stimulus position indicated at the bottom of the panel.

(D) Directional selectivity in the model; same conventions as in (B).

Dendrites with calcium-permeable ionotropic receptors (e.g., insect nAChRs; Thany et al., 2007; Oertner et al., 1999, 2001; Borst and Egelhaaf, 1992) but lacking VGCCs or release of calcium from internal stores are ideal for this approach, as the latter can spatially distort the calcium signal. Calcium imaging has been employed to study connectivity in several systems: the fly LPTCs (Borst and Egelhaaf, 1992), cricket omega neurons (Baden and Hedwig, 2007), the cricket cercal system (Ogawa et al., 2006, 2008), and the zebrafish tectum (Bollmann and Engert, 2009). In contrast to the aforementioned systems, the LGMD excitatory dendrite has the distinct advantage of having very few or no VGCCs (Peron and Gabbiani, 2009a) in conjunction with calcium-permeable nAChRs (Figure S1).

Though we demonstrated a high degree of topography preservation at both the coarse (Figures 2 and S4) and fine (Figure 3)

scales, the technical limitation of our approach means our results constitute a lower bound for wiring specificity. This is because the tips of the LGMD's dendrites are fairly deep in the tissue (up to ~ 200 μm), and are therefore difficult to resolve using our imaging approach. Despite this limitation, the precise wiring demonstrated here raises the possibility that even individual adjacent axons preserve topography. This has important consequences in the context of map development and for understanding computations performed by neurons receiving topographic projections.

Implications for Dendritic Integration

Due to the precision of the mapping and the unique morphology of the LGMD, we can interpret the responses to flashing bars and directional stimuli in the context of interbranch versus

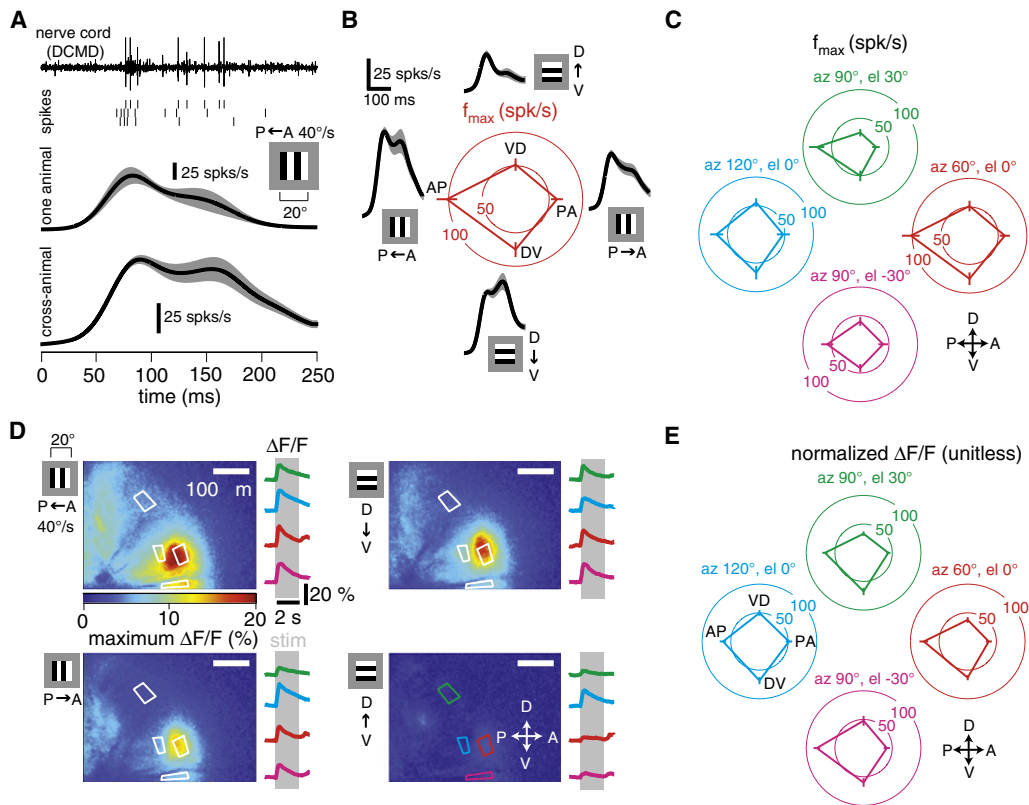


Figure 6. Both the Peak Firing Rate and Synaptic Calcium Response of the LGMD Are Directionally Selective for Local Motion Stimuli

(A) LGMD/DCMD response to drifting grating, consisting of two 5° -by- 20° black edges separated by 5° white regions moving in a 20° -by- 20° square at $40^\circ/\text{s}$ in an AP direction. To avoid net luminance change, the background luminance was 50%. The top trace shows a sample nerve cord recording with large DCMD spikes, with the raster for several trials and the Gaussian-convolved mean instantaneous frequency with SEM envelopes shown below ($n = 3$ trials). The average instantaneous frequency pooled across animals ($n = 15$ trials, three per animal) is shown below. This particular stimulus was centered in anterior visual space (azimuth 60° , elevation 0°).

(B) Directional selectivity at the level of f_{max} , with mean instantaneous frequency responses pooled across animals shown for each direction of drift for the same stimulus position as in (A). The circular plot indicates f_{max} for each direction, with the line indicating cross-animal SEM ($n = 5$).

(C) Directional selectivity at the level of f_{max} for four different stimulus positions.

(D) Sample calcium responses for all four directions of motion. For each motion direction, a sample maximal $\Delta F/F$ response to anterior (azimuth 60° , elevation 0°) stimuli is shown. The regions outlined in white correspond to the regions of interest (ROIs); on the DV motion panel, ROIs are outlined in color, corresponding to the color in which $\Delta F/F$ versus time is shown for each ROI and stimulus. Directional arrows correspond to the position in visual space of the incoming inputs from the eye (see Figure 1).

(E) Directional selectivity at the level of maximal $\Delta F/F$ within each of the four ROIs in (D). The color code corresponds to the ROI's position. For each animal-ROI combination, data was normalized to the maximal $\Delta F/F$ across stimulus classes (including those from Figure S2), and each value on the circular plot indicates the average normalized $\Delta F/F$ pooled across animals ($n = 15$ trials, over five animals; lines indicate SEM).

intrabranched summation (Polsky et al., 2004; Poirazi et al., 2003). Specifically, vertical bars, as well as AP/PA drifting gratings, should activate synapses on disparate dendritic branches, while horizontal bars and DV/VD gratings should activate synapses on adjacent branches. We observed a greater response to vertical as compared with horizontal bars, but only for larger bar sizes, consistent with passive sublinear summation due to reduced driving force. An additional observation supporting sublinear summation was that in the context of local drifting gratings, only DV motion produced a significantly lower normalized f_{max} relative to the normalized $\Delta F/F$ (Table S3). This last result is especially compelling: sublinear summation requires both clustered synaptic activity and sufficient depolarization to enter the sublin-

ear regime. DV/VD drifting gratings should stimulate synapses on the same branch, and the presynaptic DV motion preference means that the response will be much stronger than for VD motion. Most neurons studied to date employ active conductances to either compensate for passive sublinear summation (Cash and Yuste, 1998, 1999) or generate supralinear summation (Losonczy and Magee, 2006; Polsky et al., 2004; Poirazi et al., 2003); the lack of such an effect suggests that, in the context of the stimuli used in the present study, the LGMD excitatory dendrite integrates in a passive fashion. Indeed, sublinear summation caused by reduced synaptic driving force of clustered synapses has been previously postulated in the closely related fly LPTCs (Haag et al., 1992; Borst et al., 1995).

Implications for Mechanistic Understanding of Receptive Field Structure

Researchers have long postulated a role for the spatial pattern of synaptic wiring in shaping receptive fields. For instance, in visual cortex, dendritic branch asymmetry in the context of a retinotopic projection has been suggested as a mechanism for orientation selectivity (Colonnier, 1964; but see Martin and Whitteridge, 1984) as well as directional preference (Livingstone, 1998; but see Anderson et al., 1999). Our results demonstrate that interbranch versus intrabranched summation can have strong effects in the context of both static and dynamic stimuli. Thus, knowledge of subcellular connectivity can enhance our understanding of the mechanistic underpinnings of neuronal receptive fields. Recent technical advances demonstrate that it is possible to map inputs from various brain regions onto specific neuronal classes (Petreanu et al., 2009). Our work suggests that such studies can elucidate computational function, especially when dendrites sample inputs in spatially specific ways.

In the specific context of the LGMD, our work demonstrates that the cell exhibits both directional and orientation preference. Our model shows that though orientation preference is likely due to dendritic filtering, directional preference is almost certainly presynaptic. This is based on the fact that not only the firing rate but also the dendritic calcium response is strongly directionally biased. Were directional preference a consequence of dendritic filtering or due to the feedforward inhibitory inputs impinging on dendritic fields B and C (see Figure 1A), one would expect nondirectional calcium responses. In the specific case of feedforward inhibition, directional bias should result in greater hyperpolarization during nonpreferred motion. This would predict a greater calcium influx during nonpreferred motion due to increased driving force, the opposite of what was observed. Presynaptic directional preference is consistent with observations in the fly (Douglass and Strausfeld, 2003; Dürr et al., 2001; Single and Borst, 2002; Single et al., 1997), but its specific mechanism remains to be determined. As for orientation preference, our work does not rule out the involvement of mechanisms other than dendritic filtering. For instance, orientation-selective lateral inhibition presynaptic to the LGMD or orientation-selective feedforward inhibition impinging on dendritic fields B and C could produce it. Nevertheless, the observed orientation preference, previous evidence for passive integration by the excitatory dendrite (Peron et al., 2007), and the relative simplicity of our model suggest that the proposed passive dendritic integration is the most parsimonious explanation for orientation preference. This is further confirmed by the relative weakness of the orientation preference, as well as its disappearance with the smallest bars.

Computationally, it is unlikely that the weak orientation preference is employed in the context of looming stimulus detection. Directional selectivity, however, may contribute to the location invariance of the LGMD's looming response (Gabbiani et al., 2001): stimuli originating in anterior visual space activate synapses in the distal dendrites, resulting in greater electrotonic filtering (Peron et al., 2007). The opposite is true for stimuli originating in posterior visual space. However, since anterior-originating stimuli are dominated by AP motion, and posterior-originating stimuli are dominated by PA motion, directional

selectivity will counteract electrotonic filtering, potentially producing a situation where the effects of the two mechanisms balance to yield invariance to approach direction.

Subcellular input specificity is likely a property of many neurons (Spruston, 2008; Petreanu et al., 2009). Our results not only show that such specificity can be very precise, but also that the layout is a critical factor in shaping the computational properties of a neuron.

EXPERIMENTAL PROCEDURES

Dissection and Visual Stimulation

Mature female locusts (*Schistocerca americana*) were immobilized in a custom holder. During dissection, visual stimulation, and imaging, the brain was bathed in locust saline. The posterior cuticle and muscle in the head capsule were removed, as was the gut. The head was detached from the body (the nerve cords and tracheae remained intact) and rotated 90° along the medial-lateral axis, using eye striations for calibration. The left eye was covered with wax and attached to the holder, as was the cuticle around the right eye. A small metal hook elevated and stabilized the brain. The protective sheath on the optic lobe was removed; for mapping experiments, the posterior optic lobe tracheae were also removed. The holder was placed in a fixed position relative to the screen, resulting in a constant eye-screen distance of 2 cm. A Sharp XVZ-12000 (Sharp Electronics Corporation, Mahwah, NJ) projector presented stimuli at a 640-by-480 resolution (~0.25 visual °/pixel), 100 Hz refresh rate, and luminance range of 0.03 to 167 cd/m².

Four groups of stimuli were employed in the study of retinotopy: premapping (n = 5 animals; Figures 6 and S2), coarse mapping (n = 7 animals; Figures 2, S3, S4, and S8), intermediate mapping (n = 5 animals; Figures S3 and S5), and fine mapping (n = 5 animals; Figures 3 and S6). For premapping, stimuli were presented sequentially, centered at four positions (see Krapp and Gabbiani, 2005, for coordinate system conventions): anterior (azimuth, elevation: 60°, 0°), dorsal (90°, 30°), posterior (120°, 0°), and ventral (90°, -30°), with a 15 s interstimulus interval. The following stimuli were employed: 50 ms, 10°-by-10° flashes on a white background with luminance decrements of 100% ("OFF"), 50%, and 10%; 50 ms, 10°-by-10° flashes on a black background with luminance increments of 10%, 50%, and 100% ("ON"); 50 ms, 5°-by-5° and 20°-by-20° OFF stimuli; 2 s, 10°-by-10° ON and OFF stimuli; and drifting grating stimuli, 0.2 cyc/° in a 20°-by-20° area (background luminance 50%), moving at 40°/s (8 cyc/s) in AP, PA, DV, and VD directions for 1 s. Three sequences were presented per animal. For coarse mapping, 25 50-ms-long 20°-by-20° OFF stimuli were presented over a 100°-by-100° region at a 10 s interval (5–14 sequences per animal; multiple imaging depths). No two adjacent positions were activated within 40 s. The fine mapping protocol was the same as the coarse, but 0.5°-by-0.5° ON stimuli were instead presented with center-wise spacings of 2° and 4°, and the luminance range employed was 3 to 1670 cd/m². Fine stimuli were always presented in the dorsal portion of visual space (centered at 30° elevation and 90° azimuth; single imaging depth). For intermediate mapping, nine stimuli were presented, centered at the same four positions as the premapping stimuli: first, a single 50 ms, 20°-by-20° OFF stimulus was presented; next, each of the four 10°-by-10° subregions of the larger stimulus was presented with a 50 ms OFF stimulus; finally, the dorsal-anterior 10°-by-10° subregion was stimulated with four 5°-by-5°, 50 ms OFF stimuli (15 s interstimulus interval; three to five sequences per animal). To evaluate the response variability (Figure S1A), a series of eight 10°-by-10° OFF stimuli were presented to one of the animals used in the intermediate mapping and several additional animals (n = 5). These stimuli were also presented at the four positions used in premapping experiments.

Single-ommatidium stimulation was applied using a custom microscope. Stimulus spots ~2.5 μm in diameter were projected focally onto the ommatidial plane, centered on single ommatidia as viewed through the microscope (ommatidium diameter: ~25 μm). We performed a series of recordings in five animals where single-ommatidium stimuli were delivered successively to several ommatidia (~4 ommatidia per animal, 19 total). The stimulus consisted of a 1500 ms duration light pulse from a baseline of 4.07 to 2530 lux (fine

mapping ON stimulus: 6.86 to 3680 lux). Thus, each presentation consisted of both an ON and OFF stimulus.

Experiments examining the computational role of retinotopy were performed with a monitor (see Peron et al., 2007). OFF bars oriented horizontally and vertically were flashed for 50 ms, centered at elevation 0° and azimuth 90°, having sizes of 80°-by-5°, 20°-by-5°, and 10°-by-2.5°. A 1 min interstimulus interval was employed (at least five repetitions per animal; $n = 7$ animals). In another set of animals, motion stimuli consisting of translating 10°-by-10° squares moving at 40°/s were presented (Figure 5). These squares appeared on the screen for 1 min prior to motion onset and translated over a 60° track (for a total of 1.5 s of motion) in the AP, PA, DV, or VD direction (track center: elevation = 0°, azimuth = 90°; five repetitions of each stimulus per animal; $n = 7$ animals). In all cases, we compensated for declining angular resolution toward the edge of the projector or monitor screen.

Electrophysiology and Imaging

DCMD recordings were performed as described previously (Fotowat and Gabbiani, 2007). Intracellular LGMD recordings and neuronal fills with OGB-1 were performed as described previously (Peron and Gabbiani, 2009a). Intracellular recordings were carried out in discontinuous current-clamp mode (DCC; 20 kHz switching frequency). Concurrent imaging and recording was performed in two of the fine mapping experiments, but the electrode was usually withdrawn, as occasional respiratory movement would often damage the cell. Single ommatidium stimulation experiments were performed using a 3M KCl electrode solution, in either DCC mode or single-electrode discontinuous voltage-clamp mode. The LGMD was identified by correlating its spikes with those of the DCMD.

ACh (Sigma-Aldrich, St. Louis, MO) iontophoresis was performed with thick-walled electrodes (0.68/1.2 mm ID/OD; WPI) filled with 1 M ACh (in H₂O). An Axoclamp 2B amplifier (Molecular Devices, Sunnyvale, CA) was employed to provide 2 s pulses for iontophoresis, with amplitudes of +10 to +100 nA; a -10 nA holding current was applied throughout. Mecamylamine (Sigma-Aldrich) cuvettes (0.1 M) were prepared in advance and added to the bath (final concentration: ~1 mM).

The imaging setup was the same as previously employed (Peron and Gabbiani, 2009a). Fluorescent illumination was applied for the duration of all imaging experiments. For ACh iontophoresis experiments, trials were spaced every 2 min, with 10 or 20 s of imaging time per trial (2 s prestimulus, 2 s iontophoresis, 6 or 16 s poststimulus). For all mapping experiments, 50 frames (5 s) were acquired per trial, starting 1 s before the visual stimulus.

Data Analysis

Data was analyzed using MATLAB (MathWorks, Natick, MA). Throughout, the nonparametric Wilcoxon rank sum test was employed for comparisons of two independent data sets; the Wilcoxon signed rank test was employed in cases where a data set's difference from 0 was evaluated, or for comparison of paired data (Lehmann, 1974). Intracellular recordings were median-filtered (8 ms window) for computing peak depolarization, and for traces in Figure 3A.

For imaging, $\Delta F/F$ was computed by using the mean fluorescence of the first five frames as the basal fluorescence. Background-subtraction was then performed for each pixel's $\Delta F/F$ time series followed by an averaging over a 5×5 pixel area centered at the given pixel. Trials containing motion artifacts were excluded. $\Delta F/F$ time series for specific regions of interest were obtained by averaging over the indicated area. For the mapping experiments, a region of interest spanning the entire excitatory dendrite was employed (Figure S3C) so as to exclude the fluorescence change due to calcium influx near the SIZ (Peron and Gabbiani, 2009a). Pixels attaining or exceeding a threshold percentage (85%) of the maximal $\Delta F/F$ for this restricted field of view were retained. Only pixels belonging to connected groups of a minimal size (10 pixels) were used. We employed the two frames following stimulus presentation for maximal $\Delta F/F$ computation. For intermediate mapping and comparison of ON and OFF inputs, a COM was computed for each trial from suprathreshold pixels; for other mappings, COMs were computed after pooling suprathreshold pixels across trials. The 85% threshold was derived by looking for the one minimizing COM positional variability (tested: 5% to 95%, in 5% increments); an 80% threshold yielded essentially the same results. The 10 pixel criteria originated from the fact that most connected suprathreshold

pixel groups that were not dendritic were one to five pixels in size; groups ≥ 10 pixels in size were always dendritic.

The excitatory dendrites of cells employed for coarse mapping were traced manually in three dimensions to derive morphologies, based on 5 μm spaced z-stacks. In such cells, the orientation of the major axis of the excitatory dendrite (i.e., roughly spanning the dorsal-ventral axis) was computed by averaging the orientation of dendritic segments less than three branch points away from the dendrite's origin. To compute the major axis length, we projected all dendritic points onto the major axis and measured the distance between the two extremal points. In conjunction with the major axis length and angle, we employed the position of the origin to normalize COM positions across cells, allowing us to construct a normalized COM distribution. COMs were projected onto the traced morphology using a minimal distance algorithm.

To calculate the degree of topography preservation, we calculated the number of times a given COM was misaligned relative to neighboring COMs whose visual stimuli shared the same elevation or azimuth (Figure S4C). For a cell with all 25 COMs this implies eight comparisons per COM (because five COMs share a given azimuth or elevation), for a total of 200 comparisons. Since each pairwise comparison is made twice, 100 unique comparisons are possible. A completely random point distribution would be expected to produce a 50% error rate. For intermediate mappings, we used sets of four COMs (Figure S5B, inset), for a total of four unique comparisons per stimulus set. The threshold for determining if two points were within or outside of instrument noise was based on the mean of standard deviations (σ) across animals for positional displacement. Because σ was normally distributed (χ^2 goodness-of-fit test; $p < 0.01$, $n = 118$: 7 animals, ~8 positions each, with ≥ 5 trials per animal-position combination to obtain individual SDs for medial-lateral and dorsal-ventral directions, which were pooled), the distance between two COMs is well approximated by a Rayleigh distribution with parameter $\sqrt{2} \cdot \sigma$ under the null assumption that the COMs are at the same location. Thus, a distance of $3.46 \cdot \sigma$ corresponds to a 95% confidence interval that the COMs are different and was selected as our threshold.

The spontaneous synaptic currents used for input number estimation were extracted from data gathered in the 500 ms period prior to single-ommatidial stimulation and selected via a local minimum detection algorithm. Candidate events were further selected based on a threshold EPSC rise slope and minimum continuous rise and decay durations (0.5 and 1 ms, respectively). Individual events were aligned to their onsets and averaged. If a subsequent event interrupted the decay of an individual event, only the period of uninterrupted decay was used when averaging.

DCMD spikes were obtained from nerve cord recordings by thresholding. Instantaneous frequency was computed as described previously (Gabbiani and Krapp, 2006; Gaussian $\sigma = 20$ ms). The maximal frequency, f_{max} , was measured from this instantaneous frequency curve. For translating stimuli, the steady-state frequency, f_{ss} , was computed as the mean frequency from 250 ms after motion onset to motion cessation (1500 ms after onset, 1250 ms total). Directionality indices (DIs) were obtained by dividing the differences of two responses (A,B) by their sum: $DI_{A/B} = (A - B)/(A + B)$.

LGMD Simulations

A multicompartment model was employed to simulate the LGMD (Figure 5C, inset). The excitatory dendrite consisted of 20 identical branches with 20 compartments each, with a tip radius of 2 μm increasing to 5 μm at the branch base; each branch was 400 μm long. Excitatory synapses were placed on these branches, with inputs 80 μm and 320 μm from the tip originating from azimuth 40° and 140° in visual space, respectively; the elevation for the top branch was 50° and -50° for the lowest branch. Synapses were distributed uniformly. A 400 μm long basal dendrite with a 10 μm radius connected these dendrites to the main process. The main process originated at the middle of this basal dendrite, and consisted of a 200 μm long 10 μm radius segment onto which feedforward inhibitory synapses were placed (green in Figure 4B; only the 100 μm furthest from the excitatory dendrite had inhibitory synapses): a 50 μm segment tapering to a radius of 1 μm , which was maintained for 50 μm as the SIZ; and a 50 μm segment detapering to a 5 μm radius, which was maintained for the length of the 650 μm axon. With the exception of the SIZ and its associated taperings, where compartments were 10 μm long, compartments were 20 μm long.

Uniform passive properties were employed throughout, with values based on previous work (Peron et al., 2007; R_m : 4500 $\Omega \cdot \text{cm}^2$, R_i : 60 $\Omega \cdot \text{cm}$, C_m : 1.5 $\mu\text{F}/\text{cm}^2$, and E_{leak} : -65 mV). Conductances and calcium were governed by the same differential equations as reported elsewhere (Peron and Gabbiani, 2009b), though g_{max} values differed from earlier work in some cases. The dendrites were passive. The tapering around the SIZ and the SIZ itself (denoted in blue and labeled “ K_{Ca} region” in Figure 4B) was endowed with a delayed rectifier (I_{KDR} ; $g_{\text{max}} = 108 \text{ mS}/\text{cm}^2$) and a sodium conductance (I_{Na} ; $g_{\text{max}} = 270 \text{ mS}/\text{cm}^2$) for spiking as well as a VGCC (I_{Ca} ; $g_{\text{max}} = 5 \text{ mS}/\text{cm}^2$) and a calcium-sensitive potassium conductance (I_{AHP} ; $g_{\text{max}} = 250 \text{ mS}/\text{cm}^2$) to generate spike-frequency adaptation (Peron and Gabbiani, 2009a). Calcium and its extrusion were also simulated in these compartments (see Peron and Gabbiani, 2009b, for exact equations and parameters). The axon only had I_{KDR} and I_{Na} , with the same g_{max} values as in the K_{Ca} region.

Excitatory and inhibitory synapses were simulated as conductance changes governed by alpha functions, with parameters $\alpha = 0.3 \text{ ms}$, basal $g_{\text{max}} = 40 \text{ mS}/\text{cm}^2$, and $E_{\text{rev}} = 0 \text{ mV}$ for excitatory synapses and $\alpha = 3 \text{ ms}$, basal $g_{\text{max}} = 100 \text{ mS}/\text{cm}^2$, and $E_{\text{rev}} = -70 \text{ mV}$ for inhibitory synapses. Visual stimulus simulation was performed by computing which regions of visual space experienced a luminance change over a given 5 ms interval; excitatory synapses were activated in a region based on the mapping from visual space, while inhibitory synapses were clustered in a 100 μm region of the SIZ-proximal process. Excitatory and inhibitory synaptic activations were delayed by an average of 50 and 100 ms following simulated visual input; to introduce noise, synapse timing delay was jittered by a Gaussian distribution with $\sigma = 5 \text{ ms}$. Dendritic synaptic density was 1 synapse/ μm for excitatory synapses (total: 8,000 synapses) and 0.15 synapses/ μm for inhibitory synapses (total: 15 synapses). To accommodate directional selectivity at the level of input synapses, g_{max} for synapses responding to AP and DV, motion was scaled by a factor of 7 and 3, respectively; no directional selectivity scaling was applied for VD- and PA-responding excitatory synapses. For nondirectionally biased simulations, a scaling factor of 2.5 was applied to all visually stimulated excitatory synapses. Spontaneous synaptic activity was simulated for both inhibition and excitation, using synapses with a nonscalable g_{max} of 1 mS/cm^2 , and a population activity rate of 200 Hz. Each spontaneous excitatory synapse was activated at a different, random position in the excitatory dendrite, while spontaneous inhibitory synapses were positioned in the small segment of the main process where inhibition was normally applied. All simulations employed a time step of 25 μs , and were carried out in Neuron 6.2 (Hines and Carnevale, 1997) on an 8-core, 2.83 GHz Mac Pro (Apple Computer Inc., Cupertino, CA).

SUPPLEMENTAL DATA

Supplemental data for this article include nine supplemental figures and three supplemental tables and can be found at [http://www.cell.com/neuron/supplemental/S0896-6273\(09\)00692-8](http://www.cell.com/neuron/supplemental/S0896-6273(09)00692-8).

ACKNOWLEDGMENTS

This work was supported by a grant from the National Institute of Mental Health and by a training fellowship from the Keck Center for Interdisciplinary Bioscience Training of the Gulf Coast Consortia (NIBIB 5T32EB006350-02) to P.W.J.

Accepted: September 9, 2009

Published: September 23, 2009

REFERENCES

- Anderson, J.C., Binzegger, T., Kahana, O., Martin, K.A., and Segev, I. (1999). Dendritic asymmetry cannot account for directional responses of neurons in visual cortex. *Nat. Neurosci.* 2, 820–824.
- Baden, T., and Hedwig, B. (2007). Neurite-specific Ca^{2+} dynamics underlying sound processing in an auditory interneurone. *Dev. Neurobiol.* 67, 68–80.
- Bollmann, J.H., and Engert, F. (2009). Subcellular topography of visually driven dendritic activity in the vertebrate visual system. *Neuron* 61, 895–905.
- Borst, A., and Egelhaaf, M. (1992). In vivo imaging of calcium accumulation in fly interneurons as elicited by visual motion stimulation. *Proc. Natl. Acad. Sci. USA* 89, 4139–4143.
- Borst, A., Egelhaaf, M., and Haag, J. (1995). Mechanisms of dendritic integration underlying gain control in fly motion-sensitive interneurons. *J. Comput. Neurosci.* 2, 5–18.
- Burrows, M. (1996). *The Neurobiology of an Insect Brain* (Oxford: Oxford University Press).
- Cash, S., and Yuste, R. (1998). Input summation by cultured pyramidal neurons is linear and position-independent. *J. Neurosci.* 18, 10–15.
- Cash, S., and Yuste, R. (1999). Linear summation of excitatory inputs by CA1 pyramidal neurons. *Neuron* 22, 383–394.
- Chen, Y., and Chiao, C. (2008). Symmetric synaptic patterns between starburst amacrine cells and direction selective ganglion cells in the rabbit retina. *J. Comp. Neurol.* 508, 175–183.
- Colonnier, M. (1964). The tangential organization of the cortex. *J. Anat.* 98, 327–344.
- David, J.A., and Pitman, R.M. (1996). Modulation of Ca^{2+} and K^{+} conductances in an identified insect neurone by the activation of an alpha-bungarotoxin-resistant cholinergic receptor. *J. Exp. Biol.* 199, 1921–1930.
- Douglass, J.K., and Strausfeld, N.J. (2003). Retinotopic pathways providing motion-selective information to the lobula from peripheral elementary motion-detecting circuits. *J. Comp. Neurol.* 457, 326–344.
- Dürr, V., Kurtz, R., and Egelhaaf, M. (2001). Two classes of visual motion sensitive interneurons differ in direction and velocity dependency of in vivo calcium dynamics. *J. Neurobiol.* 46, 289–300.
- Euler, T., Detwiler, P.B., and Denk, W. (2002). Directionally selective calcium signals in dendrites of starburst amacrine cells. *Nature* 418, 845–852.
- Fotowat, H., and Gabbiani, F. (2007). Relationship between the phases of sensory and motor activity during a looming-evoked multistage escape behavior. *J. Neurosci.* 27, 10047–10059.
- Gabbiani, F., and Krapp, H.G. (2006). Spike-frequency adaptation and intrinsic properties of an identified, looming-sensitive neuron. *J. Neurophysiol.* 96, 2951–2962.
- Gabbiani, F., Mo, C., and Laurent, G. (2001). Invariance of angular threshold computation in a wide-field looming-sensitive neuron. *J. Neurosci.* 21, 314–329.
- Gabbiani, F., Krapp, H.G., Koch, C., and Laurent, G. (2002). Multiplicative computation in a visual neuron sensitive to looming. *Nature* 420, 320–324.
- Gabbiani, F., Krapp, H.G., Hatsopoulos, N., Mo, C.H., Koch, C., and Laurent, G. (2004). Multiplication and stimulus invariance in a looming-sensitive neuron. *J. Physiol. Paris* 98, 19–34.
- Garel, S., and Rubenstein, J.L. (2004). Intermediate targets in formation of topographic projections: inputs from the thalamocortical system. *Trends Neurosci.* 27, 533–539.
- Haag, J., and Borst, A. (2004). Neural mechanism underlying complex receptive field properties of motion-sensitive interneurons. *Nat. Neurosci.* 7, 628–634.
- Haag, J., Egelhaaf, M., and Borst, A. (1992). Dendritic integration of motion information in visual interneurons of the blowfly. *Neurosci. Lett.* 140, 173–176.
- Hauselt, S.E., Euler, T., Detwiler, P.B., and Denk, W. (2007). A Dendrite-Autonomous Mechanism for Direction Selectivity in Retinal Starburst Amacrine Cells. *PLoS Biol.* 5, e185.
- Hines, M.L., and Carnevale, N.T. (1997). The NEURON simulation environment. *Neural Comput.* 9, 1179–1209.
- Jacobs, G.A., and Theunissen, F.E. (1996). Functional organization of a neural map in the cricket cercal sensory system. *J. Neurosci.* 16, 769–784.
- Jacobs, G.A., and Theunissen, F.E. (2000). Extraction of sensory parameters from a neural map by primary sensory interneurons. *J. Neurosci.* 20, 2934–2943.
- Johnston, D., and Narayanan, R. (2008). Active dendrites: colorful wings of the mysterious butterflies. *Trends Neurosci.* 31, 309–316.

- Johnston, D., Magee, J.C., Colbert, C.M., and Cristie, B.R. (1996). Active properties of neuronal dendrites. *Annu. Rev. Neurosci.* 19, 165–186.
- Kim, I., Zhang, Y., Yamagata, M., Meister, M., and Sanes, J. (2008). Molecular identification of a retinal cell type that responds to upward motion. *Nature* 452, 478–482.
- Krapp, H.G., and Gabbiani, F. (2005). Spatial distribution of inputs and local receptive field properties of a wide-field, looming sensitive neuron. *J. Neurophysiol.* 93, 2240–2253.
- Krapp, H.G., Hengstenberg, B., and Hengstenberg, R. (1998). Dendritic structure and receptive-field organization of optic flow processing interneurons in the fly. *J. Neurophysiol.* 79, 1902–1917.
- Krichmar, J.L., Nasuto, S.J., Scorcioni, R., Washington, S.D., and Ascoli, G.A. (2002). Effects of dendritic morphology on CA3 pyramidal cell electrophysiology: a simulation study. *Brain Res.* 941, 11–28.
- Lehmann, E.L. (1974). *Nonparametrics: Statistical Methods Based on Ranks* (San Francisco: Holden-Day).
- Livingstone, M.S. (1998). Mechanisms of direction selectivity in macaque V1. *Neuron* 20, 509–526.
- London, M., and Häusser, M. (2005). Dendritic computation. *Annu. Rev. Neurosci.* 28, 503–532.
- Losonczy, A., and Magee, J.C. (2006). Integrative properties of radial oblique dendrites in hippocampal CA1 pyramidal neurons. *Neuron* 50, 291–307.
- Martin, K.A., and Whitteridge, D. (1984). The relationship of receptive field properties to the dendritic shape of neurones in the cat striate cortex. *J. Physiol.* 356, 291–302.
- Matheson, T., Rogers, S.M., and Krapp, H.G. (2004). Plasticity in the visual system is correlated with a change in lifestyle of solitary and gregarious locusts. *J. Neurophysiol.* 91, 1–12.
- Migliore, M., and Shepherd, G.M. (2002). Emerging rules for the distributions of active dendritic conductances. *Nat. Rev. Neurosci.* 3, 362–370.
- Oertner, T.G., Single, S., and Borst, A. (1999). Separation of voltage- and ligand-gated calcium influx in locust neurons by optical imaging. *Neurosci. Lett.* 274, 95–98.
- Oertner, T.G., Brotz, T.M., and Borst, A. (2001). Mechanisms of dendritic calcium signaling in fly neurons. *J. Neurophysiol.* 85, 439–447.
- Ogawa, H., Cummins, G.I., Jacobs, G.A., and Miller, J.P. (2006). Visualization of ensemble activity patterns of mechanosensory afferents in the cricket cercal sensory system with calcium imaging. *J. Neurobiol.* 66, 293–307.
- Ogawa, H., Cummins, G.I., Jacobs, G.A., and Oka, K. (2008). Dendritic design implements algorithm for synaptic extraction of sensory information. *J. Neurosci.* 28, 4592–4603.
- O'Shea, M., and Williams, J.L.D. (1974). The anatomy and output connection of a locust visual interneurone: the lobular giant movement detector (LGMD) neurone. *J. Comp. Physiol.* 91, 257–266.
- O'Shea, M., and Rowell, C.H. (1976). The neuronal basis of a sensory analyser, the acridid movement detector system. II. response decrement, convergence, and the nature of the excitatory afferents to the fan-like dendrites of the LGMD. *J. Exp. Biol.* 65, 289–308.
- Peron, S.P., and Gabbiani, F. (2009a). Spike frequency adaptation mediates looming stimulus selectivity in a collision-detecting neuron. *Nat. Neurosci.* 12, 318–326.
- Peron, S.P., and Gabbiani, F. (2009b). Role of spike frequency adaptation in shaping neuronal response to dynamic stimuli. *Biol. Cybern.* 100, 505–520.
- Peron, S.P., Krapp, H.G., and Gabbiani, F. (2007). Influence of electrotonic structure and synaptic mapping on the receptive field properties of a collision-detecting neuron. *J. Neurophysiol.* 97, 159–177.
- Peteanu, L., Mao, T., Sternson, S.M., and Svoboda, K. (2009). The subcellular organization of neocortical excitatory connections. *Nature* 457, 1142–1145.
- Poirazi, P., Brannon, T., and Mel, B.W. (2003). Pyramidal neuron as two-layer neural network. *Neuron* 37, 989–999.
- Polsky, A., Mel, B.W., and Schiller, J. (2004). Computational subunits in thin dendrites of pyramidal cells. *Nat. Neurosci.* 7, 621–627.
- Rall, W. (1970). Cable properties of dendrites and effects of synaptic location. In *Excitatory Synaptic Mechanisms*, P. Anderson and J.K.S. Jan, eds. (Oslo, Norway: Universitetesforlag), pp. 176–187.
- Rall, W., Burke, R.E., Smith, T.G., Nelson, P.G., and Frank, K. (1967). Dendritic location of synapses and possible mechanisms for the monosynaptic EPSP in motoneurons. *J. Neurophysiol.* 30, 1169–1193.
- Rind, F.C., and Simmons, P.J. (1992). Orthopteran DCMD neuron: a reevaluation of responses to moving objects. I. Selective responses to approaching objects. *J. Neurophysiol.* 68, 1654–1666.
- Rind, F.C., and Simmons, P.J. (1998). Local circuit for the computation of object approach by an identified visual neuron in the locust. *J. Comp. Neurol.* 395, 405–415.
- Rind, F.C., and Leitinger, G. (2000). Immunocytochemical evidence that collision sensing neurons in the locust visual system contain acetylcholine. *J. Comp. Neurol.* 423, 389–401.
- Ruthazer, E.S., and Cline, H.T. (2004). Insights into activity-dependent map formation from the retinotectal system: a middle-of-the-brain perspective. *J. Neurobiol.* 59, 134–146.
- Schaefer, A.T., Larkum, M.E., Sakmann, B., and Roth, A. (2003). Coincidence detection in pyramidal neurons is tuned by their dendritic branching pattern. *J. Neurophysiol.* 89, 3143–3154.
- Schlotterer, G.R. (1977). Response of the locust descending movement detector neuron to rapidly approaching and withdrawing visual stimuli. *Can. J. Zool.* 55, 1372–1376.
- Single, S., and Borst, A. (2002). Different mechanisms of calcium entry within different dendritic compartments. *J. Neurophysiol.* 87, 1616–1624.
- Single, S., Haag, J., and Borst, A. (1997). Dendritic computation of direction selectivity and gain control in visual interneurons. *J. Neurosci.* 17, 6023–6030.
- Spruston, N. (2008). Pyramidal neurons: dendritic structure and synaptic integration. *Nat. Rev. Neurosci.* 9, 206–221.
- Spruston, N., Jaffe, D.B., and Johnston, D. (1994). Dendritic attenuation of synaptic potentials and currents: the role of passive membrane properties. *Trends Neurosci.* 17, 161–166.
- Stepanyants, A., and Chklovskii, D.B. (2005). Neurogeometry and potential synaptic connectivity. *Trends Neurosci.* 28, 387–394.
- Stepanyants, A., Tamás, G., and Chklovskii, D.B. (2004). Class-specific features of neuronal wiring. *Neuron* 43, 251–259.
- Strausfeld, N.J., and Nässel, D.R. (1981). Neuroarchitecture serving compound eyes of crustacea and insects. In *Comparative Physiology and Evolution of Vision of Invertebrates B: Invertebrate Visual Centers*, H. Autrum, ed. (Berlin: Springer), pp. 1–132.
- Thany, S.H., Lenaers, G., Raymond-Delpech, V., Sattelle, D.B., and Lapied, B. (2007). Exploring the pharmacological properties of insect nicotinic acetylcholine receptors. *Trends Pharmacol. Sci.* 28, 14–22.
- Verkhatsky, A., and Shmigol, A. (1996). Calcium-induced calcium release in neurones. *Cell Calcium* 19, 1–14.
- Vetter, P., Roth, A., and Häusser, M. (2001). Propagation of action potentials in dendrites depends on dendritic morphology. *J. Neurophysiol.* 85, 926–937.
- Williams, S.R., and Stuart, G.J. (2003). Role of dendritic synapse location in the control of action potential output. *Trends Neurosci.* 26, 147–154.
- Wilson, M. (1975). Angular Sensitivity of Light and Dark Adapted Locust Retinula Cells. *J. Comp. Physiol.* 97, 323–328.